Chemical Science

ROYAL SOCIETY OF CHEMISTRY

EDGE ARTICLE

View Article Online
View Journal | View Issue

Cite this: *Chem. Sci.*, 2021, **12**, 11748

All publication charges for this article have been paid for by the Royal Society of Chemistry

Received 15th June 2021
Accepted 2nd August 2021

DOI: 10.1039/d1sc03232a

rsc.li/chemical-science

Substrate-independent three-dimensional polymer nanosheets induced by solution casting†

Cheol Hun Park,‡[a] Eun Min Go,‡[b] Kyung Min Lee,[b] Chang Soo Lee,[a] Sang Kyu Kwak*[b] and Jong Hak Kim *[a]

Nanosheets are important structures usually composed of inorganic materials, such as metals, metal oxides, and carbon. Their creation typically involves hydrothermal, electrochemical or microwave processes. In this study, we report a novel formation mechanism of 3D polymer nanosheets *via* facile solution casting using a comb copolymer consisting of poly(ethylene glycol) behenyl ether methacrylate and poly(oxyethylene) methacrylate (PEGBEM–POEM). Controlling the composition of comb copolymer yielded nanosheets with different packing density and surface coverage. Interestingly, the structure exhibits substrate independence as confirmed by glass, inorganic wafer, organic filter paper, and porous membrane. The formation of 3D nanosheets was investigated in detail using coarse-grained molecular dynamics simulations. The obtained polymer nanosheets were further utilized as templates for inorganic nanosheets, which exhibit high conductivity owing to interconnectivity, and hence have promising electronic and electrochemical applications.

Introduction

Nanostructured materials have been widely investigated owing to their unique properties arising from the nanoscale microstructure. These nanomaterials have played a pivotal role in shaping the outcome of numerous important studies, not only in the fields of physics, chemistry, and biology but also in engineering.[1–3] In general, several properties of nanomaterials, such as optical, electrical, mechanical, magnetic, and chemical, have been tuned using size-controlling technology for various applications.[4–7] Moreover, the size-dependent properties of nanomaterials have led to significant technological advancements in quantum dots, chemical catalysts, biomedical applications, and photovoltaic devices.[8–13]

The structure of inorganic materials has been controlled *via* a range of methods, such as hydrothermal, electrochemical, template mediated calcination, solvothermal, microwave, and exfoliation.[14–19] The resulting single and multi-dimensional structures have fascinating properties, and consequently, several studies have been conducted with the goal of synthesizing structures with larger specific surface area, superior activity, and higher porosity. Nanostructured materials with high aspect-ratio have garnered great attention lately, which are ultrathin materials with high crystal growth and stacked layers. Several studies have been conducted to enhance the physicochemical properties of these materials with promising results, which mainly involved inorganic materials such as graphene, two-dimensional (2D) metal organic frameworks (MOFs), and metal oxides.[20–26]

Multi-dimensional nanostructure is particularly promising in polymer engineering. As the development of specific nanostructures is not common in polymers owing to their low crystallinity and rigidity compared to inorganic materials, most polymers only exhibit indistinguishable structures in the absence of proper treatment, processing, and substrates. However, utilizing specialized techniques such as electrospinning, nonsolvent-induced phase separation, oxidizing agents, and blending with carbon materials, various nanostructures including nanowires, nanofibers, and nanospheres have been generated.[27–32] For example, polypyrrole conducting polymer with nanosheets were formed using electrochemical reactions and chemical oxidative polymerization, which resulted in an improved electrochemical performance owing to the increased specific surface area as well as a well-aligned and interconnected structure.[33–37] However, there was no report on the formation of polymer nanosheets *via* solution casting, which is a cost-effective simple process for commercialization.

In this study, we report a novel formation mechanism of polymer materials with three-dimensional (3D) nanosheets using a solution casting method. We also confirm the substrate-independent property of the 3D polymer nanosheets using

[a]*Department of Chemical and Biomolecular Engineering, Yonsei University, 50 Yonsei-ro, Seodaemun-gu, Seoul 03722, Republic of Korea. E-mail: jonghak@yonsei.ac.kr*

[b]*Department of Energy Engineering, School of Energy and Chemical Engineering, Ulsan National Institute of Science and Technology (UNIST), Ulsan 44919, Republic of Korea. E-mail: skkwak@unist.ac.kr*

† Electronic supplementary information (ESI) available. See DOI: 10.1039/d1sc03232a

‡ These authors contributed equally to this work.

glass, inorganic wafer, organic filter paper and polymer membranes as substrates. The nanosheet structure is based on a comb copolymer composed of poly(ethylene glycol) behenyl ether methacrylate and poly(oxyethylene) methacrylate (*i.e.* PEGBEM–POEM), which is synthesized *via* free-radical polymerization—a cost-effective, eco-friendly, and facile method.[38–41] Furthermore, we discuss in detail the physicochemical properties and formation mechanism of the nanosheets using coarse-grained molecular dynamics (CGMD) simulations. The 3D polymer nanosheets were also used as templates for nanosheets made of metal and other materials using coating and mixing methods.

Results

Design and characterization of the comb copolymer

The formation of 3D nanosheets *via* solution casting method is based on PEGBEM–POEM comb copolymers with different compositions synthesized using free-radical polymerization (Fig. 1a and b). Two macromonomers of PEGBEM and POEM underwent the reaction in ethyl acetate at 70 °C for 18 h. We confirmed our synthesis using various techniques, such as Fourier-transform infrared (FT-IR) spectroscopy, thermogravimetric analysis (TGA), differential scanning calorimetry (DSC), wide-angle X-ray scattering (WAXS), small-angle X-ray scattering (SAXS), and nuclear magnetic resonance (NMR). In the FT-IR spectroscopic measurement, complete polymerization was confirmed by the disappearance of the carbon double bonds at 1637 and 1632 cm^{-1} for POEM and PEGBEM, respectively (Fig. 1c). We found that as the PEGBEM content increases, the thermal stability and degree of crystallinity also increases owing to the intermolecular packing of the sequential methylene chains of PEGBEM. Specifically, the thermal degradation temperature of PEGBEM–POEM increased with the PEGBEM content and all PEGBEM–POEM comb copolymers were thermally stable up to 250 °C (Fig. 1d). The PEGBEM–POEM (7 : 3) comb copolymer exhibited the highest degree of crystallinity (Fig. 1e and f), which is because the PEGBEM chains consist of regularly aligned twenty methylenes and twenty-five ethylene oxides. The *d*-spacing between the sequential methylene chains was determined using SAXS to be approximately 9.0 nm for PEGBEM–POEM (10 : 0); however, the *d*-spacing increased to 9.8 nm for PEGBEM–POEM (7 : 3) owing to the polymerized amorphous phase of the POEM chains (Fig. 1g). The specific composition of the comb copolymer was obtained using ^{1}H-NMR measurements (Fig. 1h), which yielded a weight ratio of 58 : 42 for PEGBEM–POEM (7 : 3) and 34 : 66 for PEGBEM–POEM (5 : 5). This indicates similar reactivity of the two macromonomers to free radical polymerization.

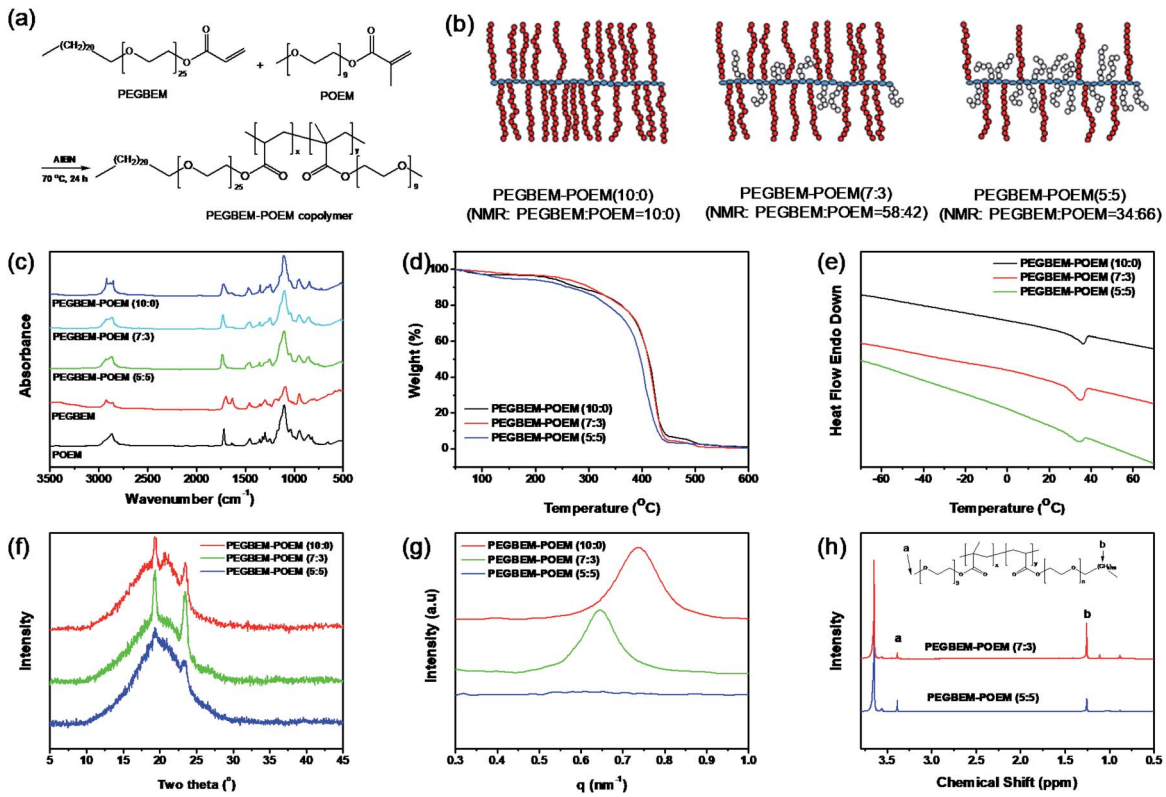

Fig. 1 Characteristics of the synthesized PEGBEM–POEM comb copolymer. (a) Synthesis scheme. (b) Schematic illustration of different polymer structures. (c) FT-IR spectroscopic measurements to confirm the polymerization. (d) TGA and (e) DSC measurements to obtain the thermal behavior. (f) WAXS measurements to determine the degree of crystallinity. (g) SAXS measurements to determine the *d*-spacing in the crystalline lattice. (h) NMR measurements to confirm the specific composition of the PEGBEM–POEM comb-like copolymer.

Formation of 3D nanosheets *via* solution casting

In this work, we mainly discuss the PEGBEM–POEM (7 : 3) comb copolymer because the 3D nanosheets were most efficiently and abundantly formed for this composition, as shown in Fig. 2. Briefly, 10 wt% PEGBEM–POEM solutions in various solvents were directly solution-casted on the substrate, and dried at an ambient condition except for less volatile solvents such as DMF and NMP. We report that the development of the structure is highly dependent on the thickness of the PEGBEM–POEM (7 : 3) film. When the film thickness was 2 μm, a dense homogeneous structure was observed, which is a common morphology of polymers developed using solution casting (Fig. 2a and b). The nanosheets started to form at a film thickness of 6 μm (Fig. 2c and d), and a large-scale 3D nanosheet structure was observed at a film thickness of 12 μm (Fig. 2e and f). Note that to investigate the effect of each polymer unit on the assembled structures, PEGBEM–POEM (10 : 0) and PEGBEM–POEM (5 : 5) were used as control samples, which will be discussed later.

Interestingly, the 3D nanosheet structure of PEGBEM–POEM (7 : 3) was observed regardless of the kind of substrate used, namely, conducting fluorine-doped tin oxide (FTO) glass, cellulose filter paper, silicon wafer, and porous polysulfone membrane, as shown in Fig. 2g–l. For all samples, ethanol was used as the solvent to dissolve the PEGBEM–POEM comb copolymer. Note that the porous and interweaved structure of cellulose filter paper, which is one of the most commonly used materials for filtration applications, was maintained even after the development of the 3D nanosheets. It suggests the presence of a highly increased surface area and hence the possibility of increased filtration performance for water treatment.

In order to consider the use in electronic and electrochemical devices, we deposited metal and metal oxides on the nanosheets. As shown in ESI, Fig. S1,† Pt was successfully sputtered on the 3D PEGBEM–POEM nanosheets without collapsing the structure. Owing to the sputtering, the thickness of the nanosheets increased from approximately 20–30 to 100 nm. To remove the PEGBEM–POEM matrix and obtain the inert 3D nanosheet structure of Pt, the Pt-sputtered sample was dipped in ethanol and calcined at 450 °C. This is because the PEGBEM–POEM (7 : 3) comb copolymer is highly soluble in ethanol and completely degrade at 500 °C, as confirmed by TGA in Fig. 1d. Note that following the ethanol treatment and annealing process, the 3D nanosheet structure was still maintained without severe shrinkage. In addition to Pt, other inorganic materials such as gold, aluminum, indium tin oxide (ITO), and graphene oxide were also coated onto the 3D polymer nanosheets, as shown in Fig. 3a–f. Note that the metal salt $Zn(NO_3)_2$ was mixed with the PEGBEM–POEM (7 : 3) solution before casting on the substrate. In general, the thickness, size and packing density of the nanosheets were influenced by the sputtering sources. Nevertheless, all the samples exhibited well-defined 3D nanosheets without any discernible collapse or distortion.

Other commercially available polymers, namely, hydrophobic poly(1-trimethylsilyl-1-propyne) (PTMSP), hydrophilic

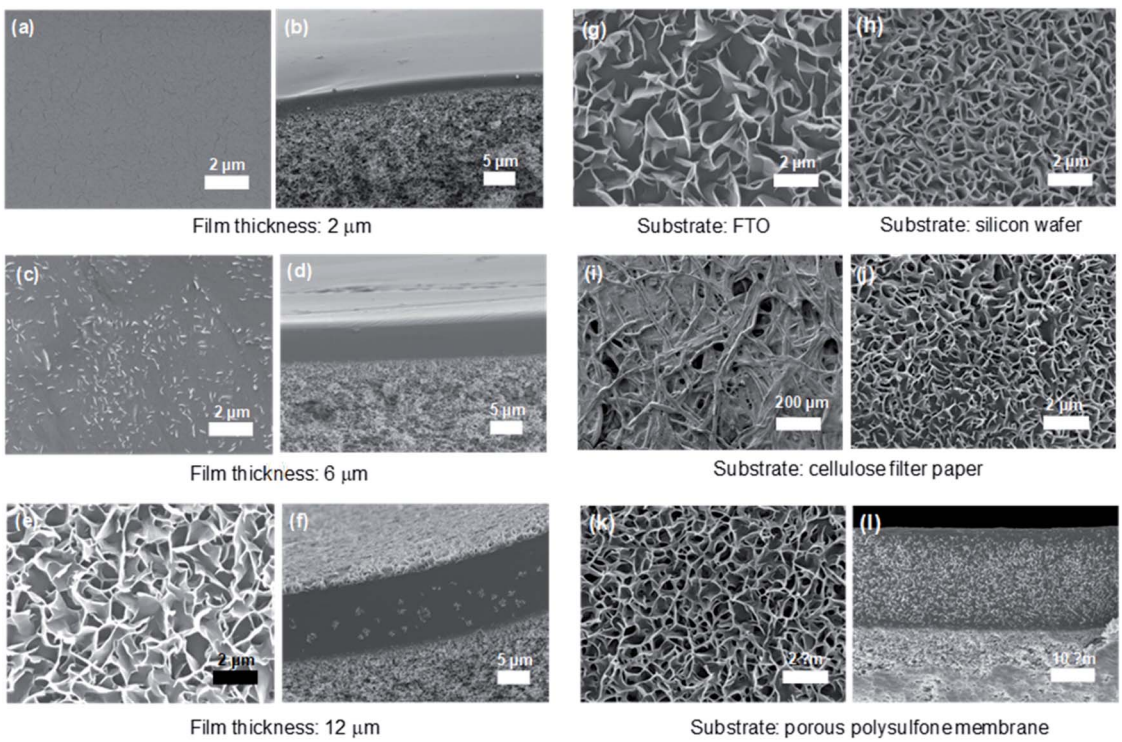

Fig. 2 Development of 3D polymer nanosheets for different thicknesses of the PEGBEM–POEM (7 : 3) film. Film thickness: (a and b) approximately 2 μm; (c and d) 6 μm; (e and f) 12 μm on the polysulfone substrate. Surface SEM images of the 3D PEGBEM–POEM (7 : 3) nanosheets on the following substrates: (g) FTO glass; (h) silicon wafer; (i and j) cellulose filter paper; (k and l) porous polysulfone membrane.

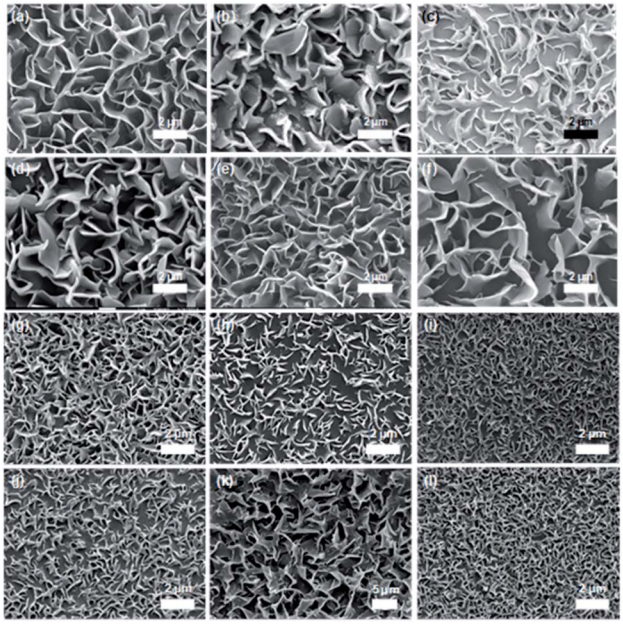

Fig. 3 SEM images of 3D PEGBEM–POEM (7 : 3) nanosheets sputtered with the following inorganic materials: (a) gold; (b) aluminum; (c) platinum; (d) indium tin oxide (ITO); (e) graphene oxide; and solution mixed with (f) $Zn(NO_3)_2$. Effect of the solvent on the development of 3D polymer nanosheets. Solvents used: (h) methanol; (h) isopropanol; (i) butanol; (j) THF; (k) DMF; (l) NMP.

poly(ethylene oxide) (PEO), amphiphilic poly(ether-block-amide) (PEBAX) block copolymer, and different kinds of comb copolymers (synthesized using the same method as PEGBEM–POEM (7 : 3)) were also prepared *via* the same method. As shown in ESI, Fig. S2,† dense and flat surfaces were observed in all cases, as expected, except for the PEGBEM–POEM comb copolymers. For PEGBEM–POEM (10 : 0) and PEGBEM–POEM (5 : 5), partially non-homogeneous regions and incompletely formed nanosheets were observed in the magnified images (see Fig. S2g and h,† respectively).

The temperature is considered to be an important factor for the development of 3D nanosheets and hence it was investigated, as shown in ESI, Fig. S3.† The solubility of PEGBEM–POEM comb copolymer in ethanol tends to increase with temperature. When the casted polymer solution was dried at a high temperature (*i.e.*, 50 °C), the surface coverage of the 3D nanosheets was significantly decreased. This resulted in the formation of mixed dense and nanosheet structures, as shown in Fig. S3a.† Identical 3D nanosheets were observed in the corresponding magnified image (see Fig. S3b†) with a low growth of nanosheets oriented along the normal condition. Contrarily, at a low temperature (*i.e.*, −15 °C), the 3D nanostructures consisted of loosely packed nanosheets of larger size as well as densely packed nanosheets that were well developed, thus exhibiting full surface coverage. Therefore, we can conclude that using lower temperatures leads to the formation of a more packed 3D structure composed of a large number of small-sized nanosheets.

The 3D nanosheets of the PEGBEM–POEM (7 : 3) film were developed using several solvents, as shown in Fig. 3g–l. As PEGBEM–POEM (7 : 3) is not soluble in non-polar solvents, a series of polar solvents was tested, such as alcohols (*i.e.*, methyl alcohol, isopropanol, and butanol) and organic solvents (*i.e.*, tetrahydrofuran (THF), *N*,*N*-dimethylformamide (DMF), and 1-methyl-2-pyrrolidinone (NMP)). When the 3D nanosheets were prepared with methanol, properties exactly similar to those obtained with ethanol were observed, such as surface coverage, sheet size, and growth, as shown in Fig. 3g. However, in the case of isopropanol, both the size of the nanosheets and the surface coverage decreased, resulting in a wider growth of nanosheets with lower packing density (see Fig. 3h). A similar behavior was also observed in the samples prepared with butanol and THF (see Fig. 3i and j). In Fig. 3k, where DMF was used as the solvent, a more interconnected and wider nanosheet structure was obtained. Meanwhile, when NMP was used (see Fig. 3l), the nanosheets shrunk and the surface coverage decreased. Moreover, the use of different kinds of solvents resulted in change in the nanosheets thickness due to different polymer–solvent interactions. We report that both the drying temperature and the kind of solvent used are pivotal parameters for the development of nanosheets, and thus, our results can lead to better optimization of the nanosheet structure depending on their specific purpose.

Computational study of the formation of nanosheets

To theoretically investigate the formation of nanosheets and dense structures, the CGMD simulation was performed (see Computational method for details).[42–47] The modeled PEGBEM–POEM comb copolymer was shown in Fig. 4a. The aggregation of PEGBEM–POEM comb copolymers was investigated at different evaporation rates of the ethanol solvent since the solvent was expected to evaporate slower in the thick film. For the formation of nanosheets, the solvent was evaporated at a rate of 1.75×10^{-8} mL s^{-1} for 1.4 μs at 288 K. Consequently, PEGBEM–POEM was aggregated during the evaporation of the solvent and the nanosheet form appeared (see Fig. 4b and ESI, Fig. S5†). For the formation of dense structures, on the other hand, PEGBEM–POEM was assembled without flat surface, (see Fig. 4c and ESI, Fig. S6†), when the solvent was evaporated at a rate of 9.8×10^{-7} mL s^{-1} for 50 ns at 310 K. At different evaporation rates, the movement of the PEGBEM–POEM comb copolymer was traced over simulation time to obtain mean square displacement (MSD). During the formation of nanosheets, the movement of PEGBEM–POEM decreased with time while it rapidly increased during the formation of dense structures (Fig. 4d). After complete removal of the solvent, the end-to-end distance of a PEGBEM chain was drastically reduced in the case of dense structures while the stretched PEGBEM chain in the nanosheets was maintained (see ESI, Fig. S7†).

To investigate this phenomenon more specifically, the solvent accessible surface area (SASA) of PEGBEM–POEM was calculated for the structures. The nanosheet structures showed much larger SASA than that in the dense ones (see Fig. 4e). In order to elucidate the difference of the SASA values, the

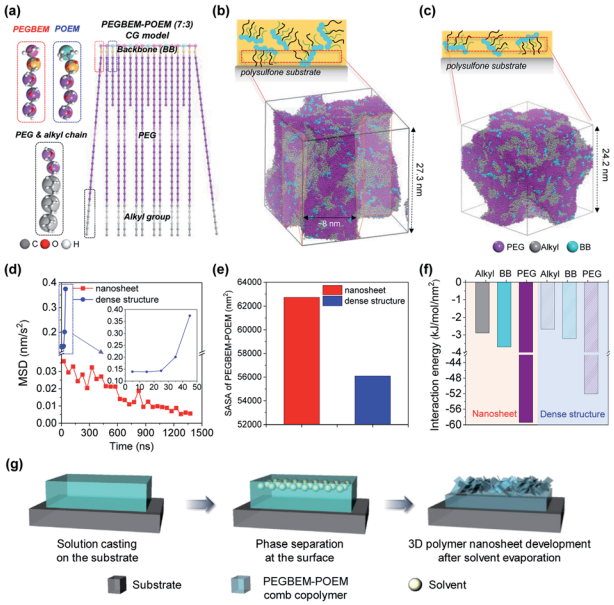

Fig. 4 CGMD simulations to analyze the formation of PEGBEM–POEM (7 : 3) nanostructures. (a) CG model of PEGBEM–POEM (7 : 3). Backbones (BBs) of PEGBEM and POEM with 3 contiguous PEG beads are shown enclosed in red and blue dotted boxes, respectively. Alkyl groups with 2 contiguous PEG beads are shown enclosed in a black dotted box. Final configurations of PEGBEM–POEM (7 : 3) (b) nanosheets and (c) dense structures obtained from CGMD simulations. The surface of the nanosheet is indicated by the orange box. (d) MSD of PEGBEM–POEM (7 : 3) in the nanosheet and dense structures as a function of the simulation time. Inset shows MSD in the dense structure. (e) SASA of PEGBEM–POEM in the nanosheet and dense structures. (f) Interaction energy per unit surface area between the solvent and components of PEGBEM–POEM during the final 20 ns of the evaporation simulation and (g) formation mechanism for 3D polymer nanosheets.

interaction tendency between PEGBEM–POEM and solvent was compared based on the interaction energy per surface area between solvent–PEGBEM–POEM. The nanosheet structures generally showed higher interaction with solvent (see Fig. 4f), which is closely relevant to its stretched structure of the PEGBEM chain (see Fig. S7†). Interestingly, among the three components of PEGBEM–POEM, weak interactions between alkyl groups and solvents were seen in both structures, but the SASA of the alkyl group only revealed less of the alkyl group in the nanosheet structure (see Fig. S8†) through slow reduction of SASA of alkyl group over time (see Fig. S9†). Thus, the slower evaporation of the solvent resulted in more reduction of alkyl group in the surface area and the nanosheet structures were maintained more stably in the polar solvent owing to less exposed non-polar alkyl groups on the surface. In conclusion from theoretical analysis, a slow evaporation of the solvent could induce a slow aggregation of PEGBEM–POEM comb copolymer, resulting in a more favorable state for maintaining the surface structure. Schematic illustration for the formation of 3D nanosheets with the comb copolymer is shown based on the theoretical analysis (Fig. 4g).

Surface and conductive properties

To find out the effect of the nanosheets on the surface properties of the film, a contact angle measurement was performed, as shown in ESI, Fig. S10.† The hydrophilicity of the PEGBEM–POEM film was measured for varying ratios of the polymer from PEGBEM : POEM (10 : 0) to PEGBEM : POEM (5 : 5). PEGBEM–POEM (10 : 0) was found to be the most hydrophilic with the lowest water contact angle of 34.2°. With increasing POEM content, the water contact angle increased to 61.5° for PEGBEM–POEM (7 : 3) and 79.5° for PEGBEM–POEM (5 : 5). The oil contact angle was expected to exhibit the opposite behavior with PEGBEM–POEM (10 : 0) having the highest oil contact angle that decreased with increasing POEM content. Interestingly, however, the oil contact angle was the highest for PEGBEM–POEM (7 : 3), which can be attributed to its 3D nanosheet structure that gives rise to a high specific surface area and hydrophobicity. The change in surface property would be of pivotal for oil/water treatment membranes.[48,49]

Another possible application of 3D nanosheets is in electronic or electrochemical devices, such as photovoltaic devices, sensors, batteries, and transistors, where the surface area and surface properties of the electronic components are important. After sputtering with inorganic conducting materials such as ITO, aluminum, and platinum, the conductivity of the 3D nanosheets was measured using a dynamic potential sweep method, as shown in ESI, Fig. S11 and Table S1.† The PEGBEM–POEM (5 : 5) film having a flat dense structure exhibited the lowest resistance and hence highest conductivity. Interestingly, the 3D PEGBEM–POEM (7 : 3) nanosheet film with much larger surface area exhibited electron conductivity comparable to the flat PEGBEM–POEM (5 : 5) film due to excellent interconnectivity. This shows that the 3D nanosheet structure does not negatively affect the electron conductivity of materials but improves the interfacial surface area of electrode, indicating their possible applications in various electronic and electrochemical devices.

Conclusions

In this study, substrate-independent polymeric 3D nanosheets were formed *via* simple solution casting. Several factors contributing to the development of the 3D nanosheet structure were investigated. We found that the 3D nanosheet structures were most well developed in PEGBEM–POEM comb copolymer. A possible mechanism for the formation of 3D nanosheets is the change in the polymer–solvent interactions on the surface. The 3D nanosheets were especially well developed when the film thickness was greater than 6 μm. Solvent evaporation yields a mixture having low solvent content and high comb copolymer content, leading to phase separation between the solvent and PEGBEM–POEM. Regions with high concentrations of PEGBEM–POEM comb chains form continuous 3D nanosheet structures, while regions with high concentrations of the solvent exhibit voids. The effect of temperature on the 3D nanosheets supports this hypothesis. At low temperatures (*e.g.*, −15 °C), where the interaction between the solvent and comb

copolymer is weak, a larger number of 3D nanosheets was developed.

The comb copolymer for developing 3D nanosheets was prepared *via* highly facile, free radical polymerization; thus, techniques such as oxidant-meditated process, hydrothermal or electrochemical treatments were not required. Sputtering metallic elements on the surface of the 3D nanosheets as well as mixing other materials with the solution containing comb copolymer also paves the way for several applications. The 3D nanosheet structure was maintained and the original unperturbed structure was exhibited after calcination for removal of the comb copolymer template. Similar 3D nanosheets were observed when using other solvents such as alcohols (methanol, IPA, and butanol) and organic solvents (DMF, THF, and NMP), although they had a slightly different structure and packing density compared to that obtained with ethanol. Finally, the formation mechanism of the 3D nanosheets was verified using CGMD simulations, which is governed by the molecular properties of PEGBEM and POEM having a specific monomer ratio.

Experimental

Materials

The monomers for the comb copolymer were poly(ethylene glycol) behenyl ether methacrylate (PEGBEM, $M_n \sim 1500$ g mol^{-1}) and poly(oxyethylene methacrylate) (POEM, $M_n = 500$ g mol^{-1}), which were purchased from Sigma-Aldrich. The initiator for the free radical polymerization was 2,2′-azobis(2-methylpropionitrile) (AIBN, 98%), which was obtained from Acros Organics. Ethyl acetate (HPLC grade) was obtained from DUKSAN and used as the solvent for polymerization. Hexane (95%, *n*-hexane) and absolute ethanol were purchased from J. T. Baker, which were used for precipitation. Whatman cellulose filter paper (pore size 0.2 μm) was purchased from Merck. The porous polysulfone membrane was kindly provided by LG chemistry. All materials were used in the inert state without further purification or modification.

Polymerization of PEGBEM–POEM

The PEGBEM–POEM comb copolymer was synthesized *via* free radical polymerization. Three kinds of PEGBEM–POEM comb copolymer were used such that the input weight monomer ratio was controlled at PEGBEM : POEM = 10 : 0, 7 : 3, and 5 : 5. All the components, including the solvent, monomers, and initiator, were put into a round flask and N_2 purging was conducted to remove any reactive gas such as oxygen or reactants that could hinder the polymerization and lead to by-products. Next, the flask was heated to 70 °C and kept for 18 h, so that the initiator could trigger the synthesis. Then, the solution was cooled to 25 °C and precipitated using *n*-hexane. The precipitation process was conducted three times to purify the final product. The obtained copolymer was kept in a vacuum oven overnight at 50 °C to remove any residual solvents. The average yield of the graft copolymer was in the approximate range 65–70 wt%.

The molecular weight and dispersity of PEGBEM–POEM comb copolymers were approximately 20 000 g mol^{-1} and 2.5, respectively. To investigate the importance of PEGBEM, another copolymer containing a phthalate and PEGBEM was synthesized in a manner similar to the PEGBEM–POEM comb copolymer.

Characterization

FT-IR spectra were obtained in the frequency range 4000–600 cm^{-1} using an Excalibur series FT-IR instrument (DIGLAS Co., Hannover, Germany). Thermal behavior of the copolymer was investigated using differential scanning calorimetry (DSC 8000, Perkin Elmer, USA) at a heating rate of 10 °C min^{-1} and thermogravimetric analysis (TGA instruments, USA). The crystallinity and micro-phase separation were studied using WAXS, carried out on a Rigaku 18 kW rotating anode X-ray generator with Cu–K radiation, and SAXS, which was conducted using 4C SAXS II beamline at the Pohang Light Source (PLS, Korea). To analyze the specific monomer ratio of the copolymer, ^{1}H-NMR was conducted using Avance 600 MHz FT NMR spectrometer (Bruker, Ettlingen, Germany) with a 600 MHz resolution. Field-emission SEM (FE-SEM, SUPRA 55VP, Germany, Carl Zeiss) was used at 15 kV after sputtering the samples with platinum at 10 mA for 60 s. The resistance of the polymer film was obtained using a dynamic potential sweep method at an electrochemical workstation.

Computational method

We have used MARTINI force field to run CGMD and construct the model systems.[42] The PEGBEM–POEM (7 : 3) comb copolymer, in which two PEGBEM and one POEM chains were repeatedly bound, was built with 33 and 11 beads, respectively (Fig. 4a). In a comb copolymer, the number of PEGBEM and POEM chains were 12 and 5, respectively. MARTINI bead types for ethyl group (BB of PEGBEM), propyl group (BB of POEM), acrylate, ethylene glycol, and butane are *SC1*, *C2*, *Na*, *SP0*, and *C1*, respectively, following Rossi *et al.*'s work.[43] For the solvent, ethanol was used with the *P1* type, where two ethanol molecules were coarse-grained into a bead. For studying the formation of nanosheets and dense structures, modeled PEGBEM–POEM comb copolymers (*i.e.*, 450 e.a.) were introduced in a simulation box of dimensions 52 × 52 × 52 nm^3, which was filled with ethanol (*i.e.*, 901 164 beads). We have performed slow and fast evaporation simulations to confirm the evaporation-driven self-assembly of PEGBEM–POEM.[44] For slow evaporation, which, we anticipated, could occur in the thick film at 288 K and 1 atm, ethanol (*i.e.*, 5%) was removed once every 50 ns and after 200 ns, the same number of ethanol was removed once every 200 ns until ethanol of 50% remained. Then, the remaining ethanol was removed and the comb copolymer model system was run till 1.8 μs. The reason for changing the evaporation rate after ethanol of 50% was removed was shown in ESI, Note and Fig. S4.† For the fast evaporation, which, we anticipated, could occur in the thin film at 310 K and 1 atm, ethanol (*i.e.*, 20%) was removed once every 10 ns and after 50 ns, the comb copolymer model system was run till 400 ns. With stabilized systems run by

the CGMD simulation, the radius of gyration (R_g), end-to-end distance, mean square displacement (MSD), solvent accessible surface area (SASA), and interaction energy were analyzed. For the CGMD simulation, the isothermal–isobaric (NPT) ensemble, where temperature and pressure were fixed with the velocity-rescaling thermostat[45] and the Parrinello–Rahman barostat,[46] respectively, was employed. The cut-off radius for the van der Waals interaction was 1.2 nm and particle mesh Ewald (PME) summation method was used for the Coulomb interaction. The time step was set at 10 fs. The GROMACS 5.0.6 package was used for the CGMD simulation.[47]

Author contributions

C. H. P. and E. M. G. equally contributed. C. H. P., S. K. K. and J. H. K. designed the research. C. H. P. performed polymer synthesis, materials characterization and morphological analysis. E. M. G. and K. M. L. performed simulations. C. H. P., E. M. G., C. S. Lee, S. K. K. and J. H. K. analyzed the data and co-wrote the paper. All authors contributed to the research and commented on the manuscript.

Conflicts of interest

There are no conflicts to declare.

Acknowledgements

S. K. Kwak acknowledges the financial support from the National Research Foundation (NRF) of Korea (2021R1A5A6002853) and computational resource from KISTI-HPC (KSC-2019-CRE-0217). J. H. Kim acknowledges the financial support from the Material & Component Technology Development Program (20010846, development of nano sized biofilter and module for virus removal) funded by the Ministry of Trade, Industry & Energy (MOTIE, Korea)

Notes and references

1 P. G. Bruce, B. Scrosati and J. M. Tarascon, Nanomaterials for rechargeable lithium batteries, *Angew. Chem., Int. Ed.*, 2008, **47**, 2930–2946.
2 J. A. Hubbell and A. Chilkoti, Nanomaterials for drug delivery, *Science*, 2012, **337**, 303–305.
3 Z. Wang, T. Wang, A. Hua, S. Ma, Z. Zhang and L. Liu, Prolonged antimicrobial activity of silver core–carbon shell nanoparticles, *Korean J. Chem. Eng.*, 2019, **36**, 1882–1889.
4 K. Ariga, T. Mori and J. P. Hill, Mechanical control of nanomaterials and nanosystems, *Adv. Mater.*, 2012, **24**, 158–176.
5 A. Puzder, A. Williamson, F. Reboredo and G. Galli, Structural stability and optical properties of nanomaterials with reconstructed surfaces, *Phys. Rev. Lett.*, 2003, **91**, 157405.
6 L. Zhang and T. J. Webster, Nanotechnology and nanomaterials: promises for improved tissue regeneration, *Nano today*, 2009, **4**, 66–80.
7 S. Zhang, H. Niu, Y. Cai, X. Zhao and Y. Shi, Arsenite and arsenate adsorption on coprecipitated bimetal oxide magnetic nanomaterials: $MnFe_2O_4$ and $CoFe_2O_4$, *Chem. Eng. J.*, 2010, **158**, 599–607.
8 Y. Bai, I. Mora-Sero, F. De Angelis, J. Bisquert and P. Wang, Titanium dioxide nanomaterials for photovoltaic applications, *Chem. Rev.*, 2014, **114**, 10095–10130.
9 A. P. Blum, J. K. Kammeyer, A. M. Rush, C. E. Callmann, M. E. Hahn and N. C. Gianneschi, Stimuli-responsive nanomaterials for biomedical applications, *J. Am. Chem. Soc.*, 2015, **137**, 2140–2154.
10 W. Wang, Y. Guo, M. Liu, X. Song and J. Duan, Porous nano-hydroxyapatites doped into substrate for thin film composite forward osmosis membrane to show high performance, *Korean J. Chem. Eng.*, 2020, **37**, 1573–1584.
11 D. Jariwala, V. K. Sangwan, L. J. Lauhon, T. J. Marks and M. C. Hersam, Carbon nanomaterials for electronics, optoelectronics, photovoltaics, and sensing, *Chem. Soc. Rev.*, 2013, **42**, 2824–2860.
12 L. M. Rossi, N. J. Costa, F. P. Silva and R. Wojcieszak, Magnetic nanomaterials in catalysis: advanced catalysts for magnetic separation and beyond, *Green Chem.*, 2014, **16**, 2906–2933.
13 Z. Yang, C.-Y. Chen, P. Roy and H.-T. Chang, Quantum dot-sensitized solar cells incorporating nanomaterials, *Chem. Commun.*, 2011, **47**, 9561–9571.
14 I. Bilecka and M. Niederberger, Microwave chemistry for inorganic nanomaterials synthesis, *Nanoscale*, 2010, **2**, 1358–1374.
15 M. K. Devaraju and I. Honma, Hydrothermal and solvothermal process towards development of $LiMPO_4$ (M= Fe, Mn) nanomaterials for lithium-ion batteries, *Adv. Energy Mater.*, 2012, **2**, 284–297.
16 J. H. Lee, C. H. Park, J. P. Jung and J. H. Kim, Worm-like mesoporous TiO_2 thin films templated using comb copolymer for dye-sensitized solar cells with polymer electrolyte, *J. Power Sources*, 2015, **298**, 14–22.
17 H. Natter and R. Hempelmann, Tailor-made nanomaterials designed by electrochemical methods, *Electrochim. Acta*, 2003, **49**, 51–61.
18 S. Salmaoui, F. Sediri, N. Gharbi, C. Perruchot and M. Jouini, Hexagonal hydrated tungsten oxide nanomaterials: hydrothermal synthesis and electrochemical properties, *Electrochim. Acta*, 2013, **108**, 634–643.
19 J. W. Seo, Y. W. Jun, S. W. Park, H. Nah, T. Moon, B. Park, J. G. Kim, Y. J. Kim and J. Cheon, Two-dimensional nanosheet crystals, *Angew. Chem., Int. Ed.*, 2007, **46**, 8828–8831.
20 G. Fang, J. Zhou, C. Liang, A. Pan, C. Zhang, Y. Tang, X. Tan, J. Liu and S. Liang, MOFs nanosheets derived porous metal oxide-coated three-dimensional substrates for lithium-ion battery applications, *Nano Energy*, 2016, **26**, 57–65.
21 E. Hosono, S. Fujihara, I. Honma and H. Zhou, The fabrication of an upright-standing zinc oxide nanosheet for use in dye-sensitized solar cells, *Adv. Mater.*, 2005, **17**, 2091–2094.

22 T. Rodenas, I. Luz, G. Prieto, B. Seoane, H. Miro, A. Corma, F. Kapteijn, F. X. L. i Xamena and J. Gascon, Metal–organic framework nanosheets in polymer composite materials for gas separation, *Nat. Mater.*, 2015, **14**, 48.

23 P. Xiong, B. Liu, V. Teran, Y. Zhao, L. Peng, X. Wang and G. Yu, Chemically integrated two-dimensional hybrid zinc manganate/graphene nanosheets with enhanced lithium storage capability, *ACS Nano*, 2014, **8**, 8610–8616.

24 E. Yoo, J. Kim, E. Hosono, H.-s. Zhou, T. Kudo and I. Honma, Large reversible Li storage of graphene nanosheet families for use in rechargeable lithium ion batteries, *Nano Lett.*, 2008, **8**, 2277–2282.

25 Z. Zhang, Y. Chen, S. He, J. Zhang, X. Xu, Y. Yang, F. Nosheen, F. Saleem, W. He and X. Wang, Hierarchical Zn/Ni-MOF-2 nanosheet-assembled hollow nanocubes for multicomponent catalytic reactions, *Angew. Chem., Int. Ed.*, 2014, **53**, 12517–12521.

26 M. Zhao, Y. Wang, Q. Ma, Y. Huang, X. Zhang, J. Ping, Z. Zhang, Q. Lu, Y. Yu and H. Xu, Ultrathin 2D metal–organic framework nanosheets, *Adv. Mater.*, 2015, **27**, 7372–7378.

27 F. Cacho-Bailo, B. Seoane, C. Téllez and J. Coronas, ZIF-8 continuous membrane on porous polysulfone for hydrogen separation, *J. Membr. Sci.*, 2014, **464**, 119–126.

28 H. Lee, M. Koo, C. Park, M. Patel, H. Han, T. H. Park, P. Kumar, W.-G. Koh and C. Park, Zwitterion-assisted transition metal dichalcogenide nanosheets for scalable and biocompatible inkjet printing, *Nano Res.*, 2020, **13**, 2726–2734.

29 J. H. Kim, Y. Choi, J. Kang, E. Choi, S. E. Choi, O. Kwon and D. W. Kim, Scalable fabrication of deoxygenated graphene oxide nanofiltration membrane by continuous slot-die coating, *J. Membr. Sci.*, 2020, **612**, 118454.

30 S. S. Shinde, G. S. Gund, D. P. Dubal, S. B. Jambure and C. D. Lokhande, Morphological modulation of polypyrrole thin films through oxidizing agents and their concurrent effect on supercapacitor performance, *Electrochim. Acta*, 2014, **119**, 1–10.

31 P. Kumar, M. Patel, C. Park, H. Han, B. Jeong, H. Kang, R. Patel, W.-G. Koh and C. Park, Highly luminescent biocompatible $CsPbBr_3$@SiO_2 core–shell nanoprobes for bioimaging and drug delivery, *J. Mater. Chem. B*, 2020, **8**, 10337–10345.

32 Y. Cho, M. Park, J. K. Kim, S. Kim, H. S. Jung and J. H. Park, Electrochemically controlled CdS@CdSe nanoparticles on ITO@TiO_2 dual core–shell nanowires for enhanced photoelectrochemical hydrogen production, *Appl. Surf. Sci.*, 2020, **505**, 144569.

33 D. P. Dubal, S. H. Lee, J. G. Kim, W. B. Kim and C. D. Lokhande, Porous polypyrrole clusters prepared by electropolymerization for a high performance supercapacitor, *J. Mater. Chem.*, 2012, **22**, 3044–3052.

34 S. Liu, F. Wang, R. Dong, T. Zhang, J. Zhang, X. Zhuang, Y. Mai and X. Feng, Dual-template synthesis of 2D mesoporous polypyrrole nanosheets with controlled pore size, *Adv. Mater.*, 2016, **28**, 8365–8370.

35 C. Xu, J. Sun and L. Gao, Synthesis of novel hierarchical graphene/polypyrrole nanosheet composites and their superior electrochemical performance, *J. Mater. Chem.*, 2011, **21**, 11253–11258.

36 X. Yang, Z. Lin, J. Zheng, Y. Huang, B. Chen, Y. Mai and X. Feng, Facile template-free synthesis of vertically aligned polypyrrole nanosheets on nickel foams for flexible all-solid-state asymmetric supercapacitors, *Nanoscale*, 2016, **8**, 8650–8657.

37 X. Zhang, J. Zhang, W. Song and Z. Liu, Controllable synthesis of conducting polypyrrole nanostructures, *J. Phys. Chem. B*, 2006, **110**, 1158–1165.

38 J. H. Lee, J. P. Jung, E. Jang, K. B. Lee, Y. S. Kang and J. H. Kim, CO_2-philic PBEM-g-POEM comb copolymer membranes: synthesis, characterization and CO_2/N_2 separation, *J. Membr. Sci.*, 2016, **502**, 191–201.

39 C. H. Park, J. H. Lee, J. P. Jung, B. Jung and J. H. Kim, A highly selective PEGBEM-g-POEM comb copolymer membrane for CO_2/N_2 separation, *J. Membr. Sci.*, 2015, **492**, 452–460.

40 C. H. Park, J. H. Lee, J. P. Jung and J. H. Kim, Mixed matrix membranes based on dual-functional MgO nanosheets for olefin/paraffin separation, *J. Membr. Sci.*, 2017, **533**, 48–56.

41 C. H. Park, J. Y. Lim, J. H. Lee, J. M. Lee, J. T. Park and J. H. Kim, Synthesis and application of PEGBEM-g-POEM graft copolymer electrolytes for dye-sensitized solar cells, *Solid State Ionics*, 2016, **290**, 24–30.

42 S. J. Marrink, H. J. Risselada, S. Yefimov, D. P. Tieleman and A. H. de Vries, The MARTINI Force Field: coarse grained model for biomolecular simulations, *J. Phys. Chem. B*, 2007, **111**, 7812–7824.

43 G. Rossi, P. Fuchs, J. Barnoud and L. Monticelli, A Coarse-grained MARTINI model of polyethylene glycol and of polyoxyethylene alkyl ether surfactants, *J. Phys. Chem. B*, 2012, **116**, 14353–14362.

44 M. C. Kim, Onset of evaporation-driven gravitational instability in a saline solution, *Korean J. Chem. Eng.*, 2021, **38**, 144–151.

45 G. Bussi, D. Donadio and M. Parrinello, Canonical sampling through velocity rescaling, *J. Chem. Phys.*, 2007, **126**, 014101.

46 M. Parrinello and A. Rahman, Polymorphic transitions in single crystals: a new molecular dynamics method, *J. Appl. Phys.*, 1981, **52**, 7182–7190.

47 D. Van Der Spoel, E. Lindahl, B. Hess, G. Groenhof, A. E. Mark and H. J. Berendsen, GROMACS: fast, flexible, and free, *J. Comput. Chem.*, 2005, **26**, 1701–1718.

48 R. Wang, X. Zhao, N. Jia, J. Cheng, L. Liu and C. Gao, Superwetting Oil/Water Separation Membrane Constructed from *In Situ* Assembled Metal–Phenolic Networks and Metal–Organic Frameworks, *ACS Appl. Mater. Interfaces*, 2020, **12**, 10000–10008.

49 Y. Sun, R. Zhao, Q. Wang, Y. Zheng, G. Li, D. Sun, T. Wu and Y. Li, Superwetting TiO_2-decorated single-walled carbon nanotube composite membrane for highly efficient oil-in-water emulsion separation, *Korean J. Chem. Eng.*, 2020, **37**, 2054–2063.